ACS APPLIED MATERIALS & INTERFACES

Research Article

www.acsami.org

Silicide Formation Process of Er Films with Ta and TaN Capping Layers

Juyun Choi,[†] Seongheum Choi,[†] Jungwoo Kim,[†] Sekwon Na,[†] Hoo-Jeong Lee,[†] Seok-Hee Lee,[‡] and Hyoungsub Kim*,[†]

[†]School of Advanced Materials Science and Engineering, Sungkyunkwan University, Suwon 440-746, Korea

[‡]Department of Electrical Engineering, KAIST, Daejeon 305-701, Korea

Supporting Information

ABSTRACT: The phase development and defect formation during the silicidation reaction of sputter-deposited Er films on Si with ~20-nm-thick Ta and TaN capping layers were examined. TaN capping effectively prevented the oxygen incorporation from the annealing atmosphere, which resulted in complete conversion to the $ErSi_{2-x}$ phase. However, significant oxygen penetration through the Ta capping layer inhibited the $ErSi_{2-x}$ formation, and incurred the growth of several Er−Si−O phases, even consuming the $ErSi_{2-x}$ layer formed earlier. Both samples produced a number of small recessed defects at an early silicidation stage. However, large rectangular or square-shaped surface defects, which were either pitlike or pyramidal depending on the capping layer identity, were developed as the annealing temperature increased. The origin of different defect generation mechanisms was suggested based on the capping layer-dependent silicidation kinetics.

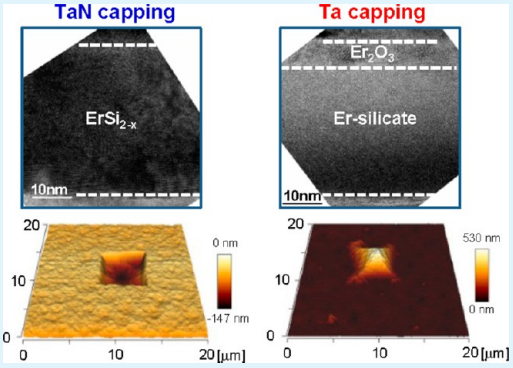

KEYWORDS: *Er-silicide, capping layer, surface defect, Ta, TaN*

1. INTRODUCTION

As a silicide-forming rare earth (RE) metal, Er has attracted a great deal of interest because its silicide phase ($ErSi_{2-x}$) has an extremely low Schottky barrier height (<0.3 eV) with respect to n-type Si.[1] Its unique material characteristics are particularly attractive for source/drain contact applications in both conventional metal-oxide-semiconductor field-effect transistors (MOSFETs) and Schottky barrier MOSFFETs.[2,3] However, the most difficult challenge from a process point of view is that it is extremely vulnerable to oxidation during the silicide-forming annealing process in an inert gas atmosphere, in which a small amount of residual oxygen still exists. As a consequence, Er is deposited under high vacuum conditions with oxidation-preventing capping layers, such as Ti,[4−8] TiN,[9,10] Mo,[11] W,[12] and amorphous-Si.[13−15] Ultrahigh vacuum (UHV) annealing can be another possible route to preventing the detrimental oxidation of Er,[3,16] but it may not be a cost-effective solution for industrial device fabrication.

Another problem with $ErSi_{2-x}$ is the large number of surface defects that appear during the silicidation reaction. Typically, on a single-crystalline (100)-oriented Si wafer, these defects have a square or a rectangular shape surrounded by four Si <100> edges, and they follow the crystallographic direction of the underlying single crystalline Si. Depending on the sample structure and annealing conditions, the apex of the defect points in either the downward direction (making them pits or pinholes[7,11,13−16]) or the upward direction (making them pyramidal defects[9,17]) on the Si substrate. Several researchers found that the surface defect density could be minimized by preamorphizing the Si substrate,[10,17] or by using a specific capping layer.[4,12−14]

Many reports have addressed the oxygen incorporation,[4,6] and have suggested several defect formation mechanisms during the Er-silicidation process.[9,11,13,15,16] Because these studies were carried out using one type of capping layer with different experimental conditions regarding the deposition method, annealing atmosphere, and capping layer, different types of defects were observed, and the origin of each defect formation has still been in debate.

In this study, for more clarification of the capping layer-dependence of the Er-silicidation process and surface defect formation, Ta and TaN, which showed different degree of oxygen permeability, were used as capping layers with identical thickness. First, the temperature-dependent Er-silicide formation kinetics were studied with differently capped and sputter-deposited Er films using various characterization tools. Finally, the differently evolving surface defects were examined with each capping layer, and attempt was made to unravel the underlying physical mechanism on the basis of the observed silicidation kinetics.

Received: September 23, 2013
Accepted: November 18, 2013
Published: November 18, 2013

2. EXPERIMENTAL SECTION

For the deposition of Er films, n-type Si (100) substrates with a resistivity of 5−15 Ω·cm were thoroughly cleaned in a hydrogen fluoride (HF) solution (HF/H_2O = 1:100) to remove native oxide, and were immediately loaded into a load-lock chamber. The base pressure of the DC magnetron sputtering chamber was ~2.3×10^{-7} Torr. An Er target with a purity of 99.95% was sputtered at a working pressure and power of ~4 mTorr and 30 W, respectively, to form ~30-nm-thick Er films. Subsequently, the capping layers with a thickness of ~20 nm were deposited in situ using TaN (99.5%) and Ta (99.99%) targets at a sputtering power of 100 W. To initiate the Er-silicidation reaction, all the samples were annealed at different temperatures ranging from 300 to 700 °C for 1 min using a rapid thermal annealing system. In order to minimize the amount of residual oxygen,[6] the chamber was pumped down for 10 min and purged by flowing high purity N_2 (99.999%) gas for 5 min before annealing. During annealing, a high purity N_2 flow was continuously applied to maintain a process pressure of ~1 Torr.

After sample preparation, the development of crystalline phases was characterized by an X-ray diffractometer equipped with a Cu Kα X-ray source (XRD, PANalytical, X'pert PRO-XPD, located at the Korea Basic Science Institute, Daegu, Korea). Detailed cross-sectional microstructural analysis was performed by transmission electron microscopy (TEM, JEOL, JEM 2100F) at 200 keV. In addition, the depth profiling mode in X-ray photoelectron spectroscopy was employed to examine the detailed phase evolution and possible oxygen incorporation during annealing (XPS, Thermo Fisher Scientific, ESCALAB 250 XPS system, located at the Korea Basic Science Institute, Busan, Korea). The XPS system used a monochromatic Al Kα source and an Ar^+ ion gun for analysis and sputter etching, respectively. The density and shape of the surface defects formed during the silicidation process was monitored by scanning electron microscopy (SEM, JEOL, JSM 7000F) and atomic force microscopy (AFM, JPK, NanoWizard3). For the detailed microstructural analysis of the formed defects, cross-sectional TEM samples were also prepared from selected annealed samples by a focused ion beam system (FIB, SII, SMI 3050TB) and imaged by TEM.

3. RESULT AND DISCUSSION

3.1. Temperature and Capping Layer Dependence of Er-Silicidation Kinetics. Figure 1 shows the XRD patterns obtained after annealing the Er films with ~20-nm-thick TaN and Ta capping layers at different temperatures, including the as-deposited sample. For the as-deposited samples and those annealed at 300 °C, a metallic Er phase was mostly identified without the formation of Er-silicide phase. In contrast to the TaN-capped sample, the as-deposited Ta-capped sample exhibited an additional peak located at 2θ = 30.2° ($d \approx 2.96$ Å), and its intensity slightly increased after annealing at 300 °C. Reckinger et al.[5] observed the appearance of a similarly located peak during the annealing of Ti-capped Er film on Si at an identical temperature, and attributed it to an oxygen-deficient ErO_x phase.[18] This suggests possible oxygen diffusion in the Ta-capped sample during the low temperature annealing and even during the exposure to air atmosphere, eventually reaching the underlying Er film. During the Er-silicidation process at low temperatures less than 500 °C, Si is known to diffuse toward the Er film and to produce an amorphous mixed layer until a sufficient number of Si atoms is supplied to form a crystalline Er-silicide phase ($ErSi_{2-x}$).[8] The early silicidation kinetics at low temperature matched well with the observed trend of the XRD spectra, in which an abrupt decrease in the Er peak and a gradual increase in the peak height of hexagonal $ErSi_{2-x}$ are observed with increases in the annealing temperature, regardless of the capping layer.

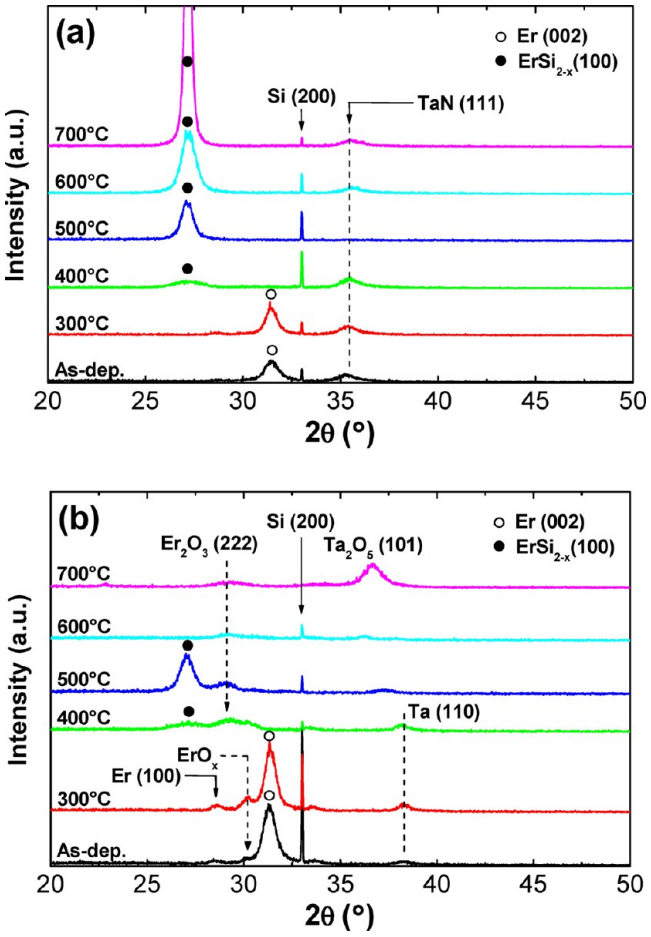

Figure 1. XRD spectra of (a) TaN-capped and (b) Ta-capped Er films on Si as a function of the annealing temperature.

However, after the onset of crystallized Er-silicide formation at 400 °C, the XRD patterns disclosed different phase-evolving paths for each differently capped sample. For the TaN-capped sample, only the $ErSi_{2-x}$ phase was generated, and its XRD peak intensity continuously increased until the annealing temperature reached 700 °C, as shown in Figure 1a, which demonstrates minimal oxygen contamination as well as excellent thermal stability. For the Ta-capped sample shown in Figure 1b, rather broad peak features were identified between (100) $ErSi_{2-x}$ and (002) Er peaks after annealing at 400 °C, accompanied by the $ErSi_{2-x}$ formation. Similar to the work of Reckinger et al.,[5] these results may be associated with several Er-oxide phases, such as Er_2O_3 and ErO_x, because of the large incorporation of oxygen atoms in the annealing atmosphere. A more significant amount of oxygen diffusion at a higher temperature over 600 °C incurred an abrupt disappearance of the $ErSi_{2-x}$ peak, while a small amount of Er_2O_3 phase remained. After annealing at the highest annealing temperature of 700 °C, a Ta_2O_5 (101) peak appeared, which also indicates facile oxygen incorporation in the Ta film.

To look closely into the microstructural and phase evolution with different capping layers, cross-sectional high-resolution TEM (HRTEM) images were taken of the differently capped Er samples after annealing at 500 and 600 °C, which are temperatures where the most critical change of the XRD patterns was exhibited. These images are displayed in Figure 2. According to the well-established silicidation kinetics of Er film,[8] Si atoms are known to be a major diffuser and form an

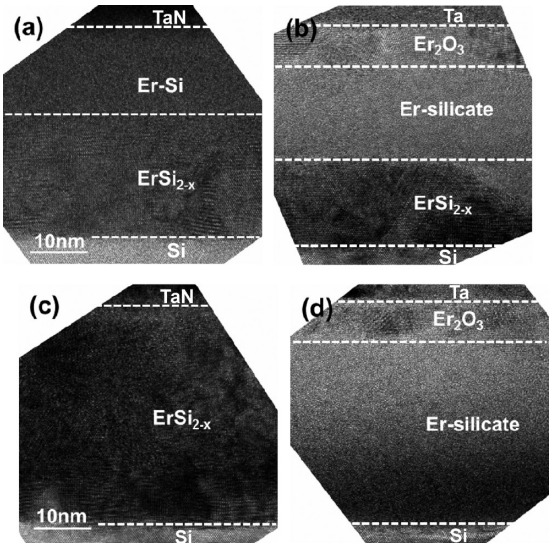

Figure 2. Cross-sectional HRTEM images of (a, c) TaN-capped and (b, d) Ta-capped Er films on Si annealed at different temperatures: (a, b) 500 °C and (c, d) 600 °C.

amorphous Er−Si mixture, even during the Er deposition step, which is followed by the nucleation of a crystalline $ErSi_{2-x}$ phase at the interface between the Er−Si mixed layer and Si substrate. Considering these well-known silicidation kinetics as well as the observed XRD spectra shown in Figure 1a, two layers observed in the TEM image of the TaN-capped sample annealed at 500 °C (Figure 2a) could be ascribed to the underlying crystalline $ErSi_{2-x}$ film and the overlying amorphous Er−Si mixed layer. In contrast to the TaN-capped sample, the Ta-capped sample had a much smaller thickness of the $ErSi_{2-x}$ layer, and an additional crystalline layer was identified on top of the amorphous layer, as shown in Figure 2b. This top crystalline layer may mostly consist of Er_2O_3, judging from the XRD indexing result in Figure 1b. Combining the XRD and TEM analysis results, it can be postulated that a significant amount of inward oxygen diffusion occurred in the Ta-capped sample, and it formed a crystalline Er-oxide phase and delayed the $ErSi_{2-x}$ growth during the annealing process. Therefore, the amorphous layer formed in the middle of the whole film structure is not expected to be a pure Er−Si mixed state, but an Er−Si−O mixed state (probably Er-silicate), which was observed in other experiments using a Ti capping layer,[4,6] and is also confirmed by the following XPS analysis.

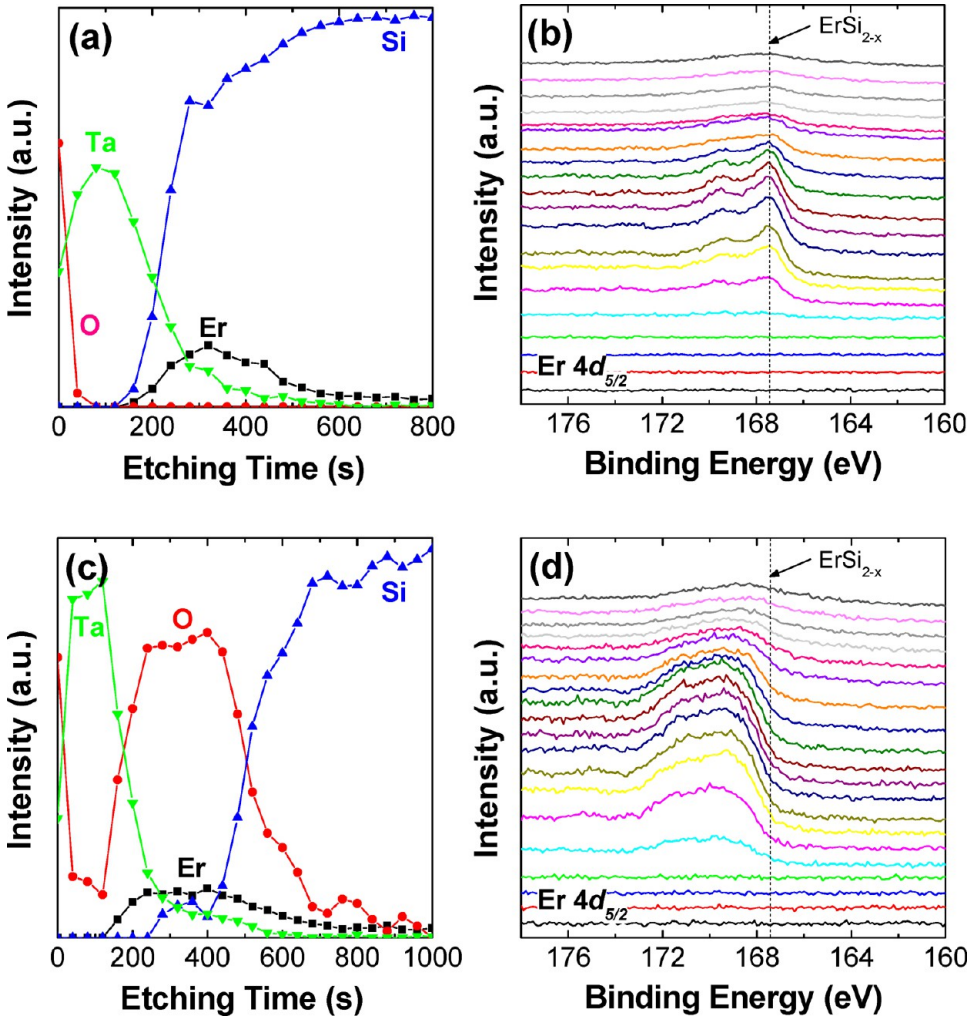

Figure 3. XPS depth intensity profiles of (a) TaN-capped and (c) Ta-capped Er films on Si after annealing at 600 °C. (b, d) The series of Er 4d XPS spectra recorded during the depth profiling of TaN-capped and Ta-capped samples, respectively. The smaller peak located at a higher binding energy of the Er $4d_{5/2}$ in (b) is a satellite peak.

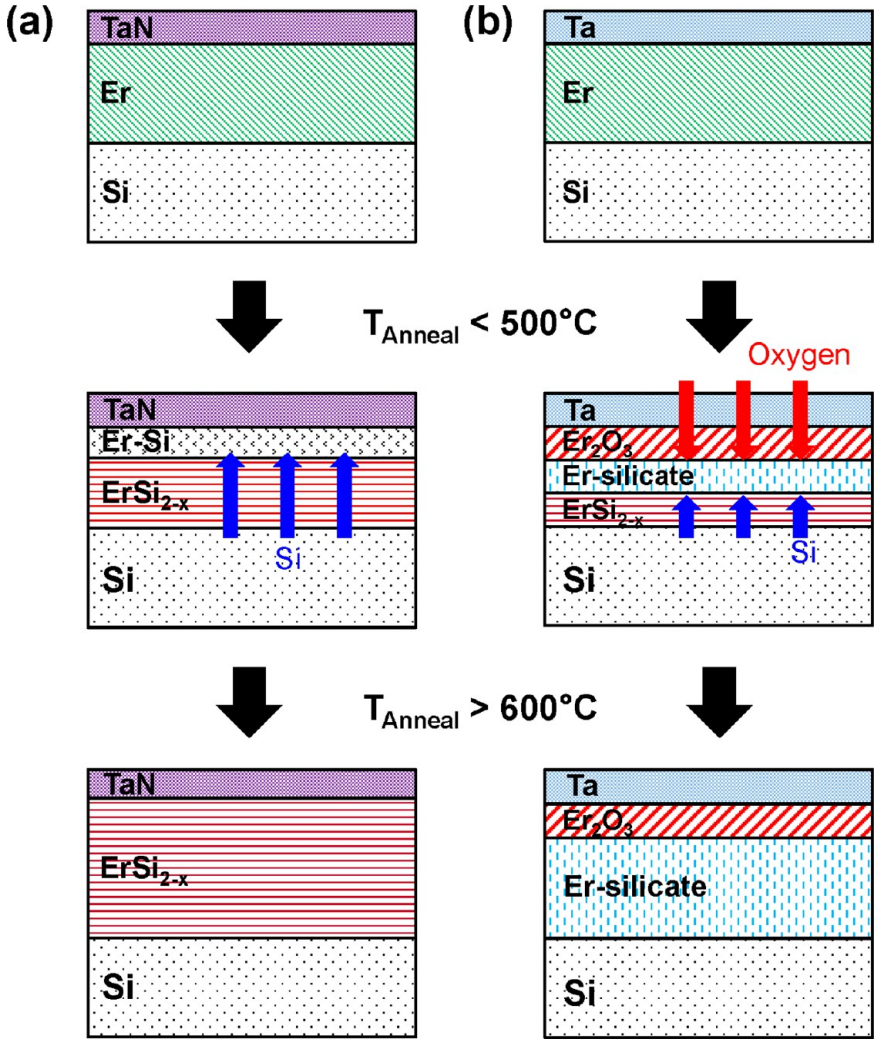

Figure 4. Schematic illustration showing the silicidation processes of (a) TaN-capped and (b) Ta-capped Er films on Si as a function of the annealing temperature.

After annealing at a higher temperature of 600 °C, an almost complete conversion of the Er−Si mixed layer into crystalline $ErSi_{2-x}$ was achieved in the TaN-capped sample with a sufficient supply of Si atoms from the substrate (Figure 2c), coinciding with the XRD results shown in Figure 1a. For the Ta-capped sample, a continuous increase in the thickness of the middle-positioned amorphous Er-silicate was observed while consuming both the overlying Er_2O_3 and underlying $ErSi_{2-x}$ layers, as shown in Figure 2d. Most of the $ErSi_{2-x}$ was consumed to form the Er-silicate layer at 600 °C, probably due to a higher rate of oxygen diffusion than that of Si out-diffusion.

The different phase evolution between the TaN-capped and Ta-capped samples associated with different degrees of oxygen diffusion was further confirmed by the XPS measurement in depth profiling mode. Figures 3a and 3c show the XPS intensity depth profiles obtained from the samples annealed at 600 °C. According to the depth profile of the TaN-capped sample shown in Figure 3a, the oxygen diffusion was effectively blocked by the TaN capping layer, and facile Si-diffusion into the Er layer was confirmed. A series of high-resolution XPS spectra of Er 4d core levels recorded during the depth profiling (Figure 3b) also corroborated the formation of a pure $ErSi_{2-x}$ phase, exhibiting an Er $4d_{5/2}$ peak located at a binding energy of ~167.4 eV throughout the entire Er-containing layer. In contrast to the TaN-capped sample, the corresponding XPS depth profile in the Ta-capped sample revealed a large amount of oxygen incorporation in the Er-containing layer with much less Si out-diffusion, as shown in Figure 3c. Furthermore, the Er $4d_{5/2}$ features shown in Figure 3d exhibited a broad spectrum shifted to a higher binding energy throughout the whole Er-containing film. The binding energies of Er $4d_{5/2}$ in Er_2O_3, ErO_x, and $ErSi_xO_y$ are reported to be higher than that of $ErSi_{2-x}$.[6] Therefore, although the detailed phase identification through the peak deconvolution process was not possible, it can be concluded that most of the Er-containing layer in the 600 °C-annealed Ta-capped sample consisted of a largely oxygen-containing film rather than pure $ErSi_{2-x}$, which further supports the disappearance of the crystalline $ErSi_{2-x}$ layer observed in the TEM analysis of Figure 2d.

On the basis of the various characterization results, a complete picture of the Er-silicidation process depending on both the annealing temperature and capping layer is schematically depicted in Figure 4. For the oxygen impermeable TaN-capped sample (Figure 4a), a continuous Si out-diffusion produced an amorphous Er−Si mixed layer first, and a crystalline $ErSi_{2-x}$ film nucleated from the interface region in contact with the Si substrate at an annealing temperature less than 500 °C. A complete transformation of the whole Er film

dx.doi.org/10.1021/am4041338 | ACS Appl. Mater. Interfaces 2013, 5, 12744−12750

into $ErSi_{2-x}$ film was achieved at over ~600 °C, followed by an improvement of the crystallinity as the annealing temperature was further increased. Alternatively, if the capping layer (in this case, ~20-nm-thick Ta film) is somewhat permeable to ambient oxygen atoms, the inward oxygen diffusion competes with the Si out-diffusion and inhibits the $ErSi_{2-x}$ growth, which results in the formation of a triple-layered structure composed of Er_2O_3/Er-silicate/$ErSi_{2-x}$ at 500 °C. A further increase in the annealing temperature over 600 °C induced a gradual growth of the amorphous Er-silicate layer by consuming the formed Er_2O_3 and $ErSi_{2-x}$ layers due to the concurrent oxygen and Si diffusion with opposite directions.

3.2. Temperature and Capping Layer Dependent Defect Formation. As discussed in the Introduction, two different types of surface defects have been observed when forming Er-silicide film on a (100)-oriented Si wafer: square or rectangular-shaped defects in either recessed (pits or pinholes[7,11,13−16]) or protruding (pyramidal defects[9,17]) forms. To investigate the capping-layer-dependent defect formation based on the different silicidation kinetics discussed thus far, the surfaces of both TaN-capped and Ta-capped samples were carefully observed after annealing at various temperatures. Figure 5 shows the tilted SEM surface images of the samples

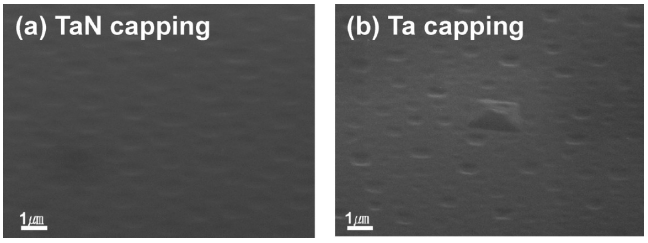

Figure 5. Tilted SEM images of (a) TaN-capped and (b) Ta-capped Er films on Si after annealing at 450 °C, which demonstrate the appearance of the recessed defects at an early stage of $ErSi_{2-x}$ formation on both samples.

after annealing at 450 °C, which is a temperature that corresponds to an early stage of the $ErSi_{2-x}$ film growth according to the afore-discussed microstructural analysis results. Both samples contained many small, recessed spots on the surface, and only the Ta-capped sample exhibited a few small protruding defects.

As the annealing temperature was further increased up to 600 °C, at which complete conversion of the Er film to $ErSi_{2-x}$ in the TaN-capped sample takes place, a completely different surface morphology started to appear on the differently capped samples. For the TaN-capped sample, the recessed defects grew further and developed into a square or rectangular shape following the crystallographic directions of the underlying Si substrate, as shown in Figure 6a. Meanwhile, the Ta-capped sample exhibited an increase in the number of protruding pyramidal defects with a distinctive size increase, while maintaining the small recessed defects (Figure 6b). In terms of the areal density of the dominant large defects, a somewhat lower density was measured on the TaN-capped sample, as compared to that on the Ta-capped sample. Further characterization of the dominating large defects was carried out by taking AFM and cross-sectional TEM images, as shown in Figure 6. Although their sizes vary substantially with a wide distribution function, the protruding defects in the Ta-capped samples were somewhat bigger than the recessed ones in the TaN-capped sample.

Various possible origins have been suggested in regard to the recessed or protruding defects observed in the samples.[9,11,13,15,16,19,20] One suggestion involves local retardation of the Si out-diffusion, which induces a nonuniform areal distribution of the silicidation rate. The local blocking of Si diffusion was explained either by the existence of residual contaminant patches on the Si wafer even after the surface cleaning prior to the RE metal deposition,[15,16] or by the formation of epitaxial RE-silicide islands at the Si interface during early silicidation stages.[11,13,19] However, the first attribution may not be plausible due to excessive size of the contaminant patches considering the thorough native oxide-cleaning procedures. In addition, Tsai et al. demonstrated that these defects were generated even in UHV annealing conditions on atomically clean Si.[13] Similar to works by Reckinger et al.[5] and Luo et al.,[11] the sporadic island growth of $ErSi_{2-x}$ was also observed instead of the layer-by-layer growth mode according to the series of HRTEM analyses of the TaN-capped samples annealed at 405 and 410 °C, as shown in Figure 7. Another origin closely related to the build-up of a biaxial compressive stress was suggested, either by the volumetric expansion during the silicidation process[20] or the epitaxial misfit between $ErSi_{2-x}$ and Si.[9]

After considering these aspects in addition to the established silicidation kinetics, the differently evolving defect formation of TaN-capped and Ta-capped samples is suggested as follows and schematically depicted in Figure 8. At a relatively low annealing temperature larger than 400 °C, an ultrathin $ErSi_{2-x}$ layer starts to nucleate at the Si interface region as discontinuous islands in both TaN-capped and Ta-capped samples, following the formation of an amorphous Er−Si mixed layer by a sufficient amount of Si diffusion into the Er film. Because there are a number of small regions without $ErSi_{2-x}$ between these islands, a large Si diffusion flux can be focused locally due to the smaller amount of Si diffusion via the surrounding crystalline $ErSi_{2-x}$ layer.[13] As a consequence, a large number of small, recessed defects may be generated independently of the capping layer identity. This may relieve the compressive stress built by the formation of $ErSi_{2-x}$, which has a larger molar volume and thermal expansion coefficient that are ~1.7 times larger than Er,[21] and more than three times larger than that of Si,[22] respectively.

However, when the annealing temperature was increased further and the oxygen diffusion became significant, especially in the Ta-capped sample, the large, recessed, and protruding defects following the crystalline direction of the underlying Si substrate start to be predominant on the TaN-capped and Ta-capped sample surfaces, respectively. For the TaN-capped sample, significant growth of the recessed defects occurred, which was probably because of the further growth of the $ErSi_{2-x}$ film with a larger volume expansion and the resulting biaxial compressive stress, which is not affected by the oxygen diffusion at all owing to the effective oxygen blocking by the TaN-capping layer. In the case of the Ta-capped sample, a new type of protruding defect (pyramidal defects) was additionally generated as the annealing temperature increased, while the recessed surface pits still remained. Tan et al.[9] attributed the origin of the protruding defects to the build-up of biaxial compressive stress by the epitaxial misfit stress between $ErSi_{2-x}$ and Si. However, according to the present experiment, although the TaN-capped sample formed a much thicker $ErSi_{2-x}$ film, no

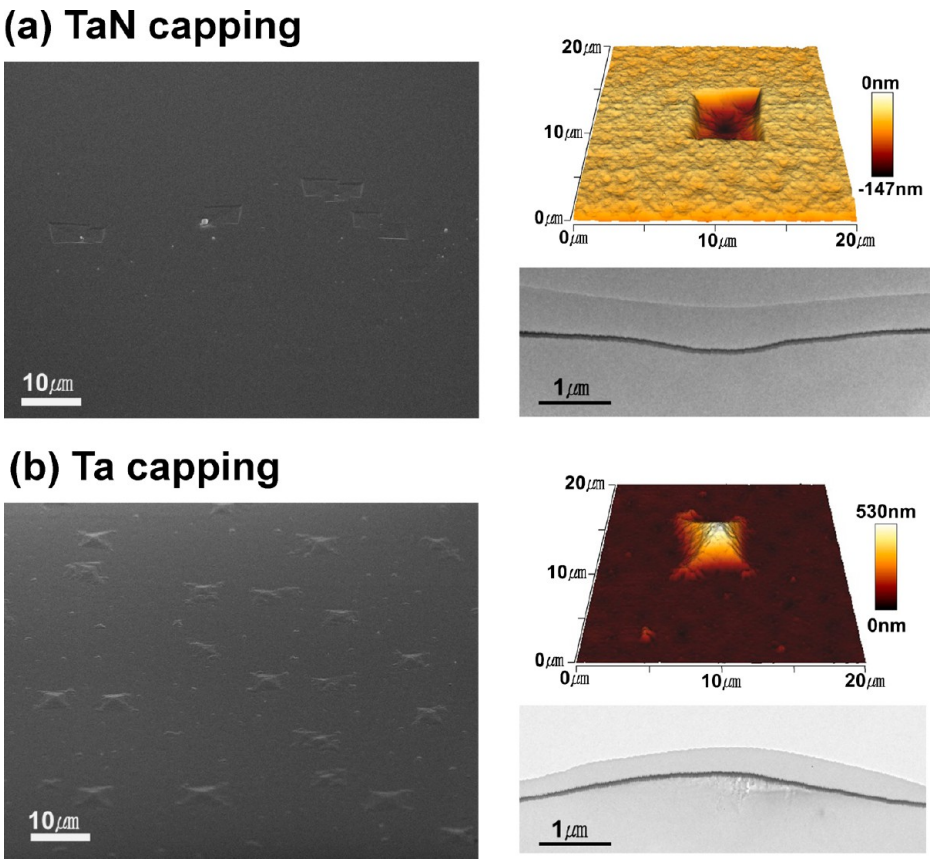

Figure 6. Tilted SEM, AFM, and cross-sectional TEM images of dominating large surface defects formed on (a) TaN-capped and (b) Ta-capped Er films on Si after annealing at 600 °C, revealing their different orientation and areal density.

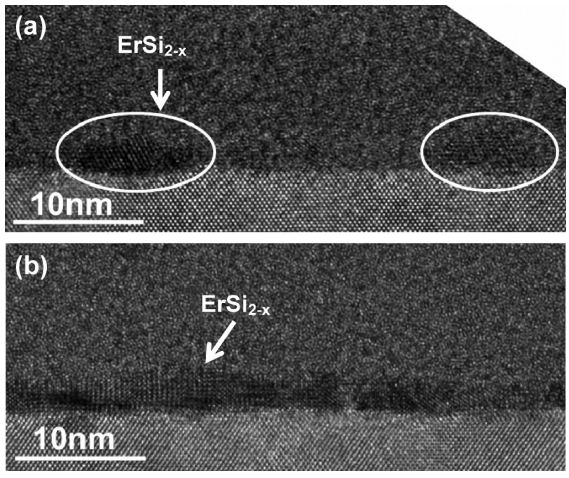

Figure 7. Cross-sectional HRTEM images of TaN-capped Er films annealed at (a) ~405 °C and (b) ~410 °C, respectively, which confirmed the island growth of epitaxial $ErSi_{2-x}$ films.

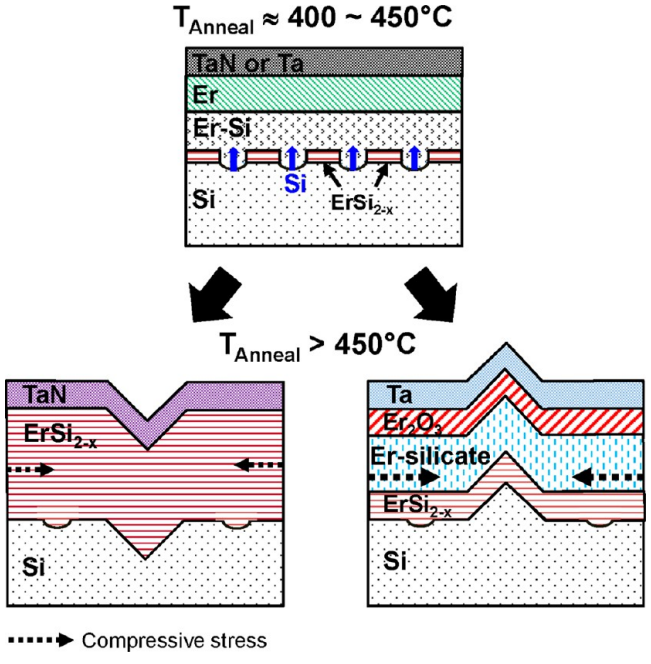

Figure 8. Schematic illustration showing the suggested model of surface defects developing as a function of the annealing temperature with different capping layers.

protruding defects were formed, which contradicts the suggested model. Various characterizations discussed in the previous part revealed that significant oxygen in-diffusion occurred along with the Si out-diffusion only in the Ta-capped sample, which evidenced the formation of oxygen-containing layers, such as Er_2O_3 and Er-silicate on top of $ErSi_{2-x}$. Therefore, the origin of the protruding defects is likely to have a direct relationship with the oxygen incorporation in the Er-containing layer. Although the molar volume of Er_2O_3 is ~1.2 times larger than that of Er,[21] and its thermal expansion coefficient is 2−3 times bigger than that of Si,[23] they are smaller than those of $ErSi_{2-x}$. Therefore, the dominant volume expansion may occur in the Er-silicate layer, which contains

dx.doi.org/10.1021/am4041338 | ACS Appl. Mater. Interfaces 2013, 5, 12744−12750

additional Si−O bonds in the Er-silicide matrix. It may build an excessive in-plane compressive stress in addition to the $ErSi_{2-x}$ film, and result in the buckling of the whole film structure. In addition, according to similar experiments using other oxygen-permeable capping materials (Ti and TiN) with different degrees of oxygen diffusion, the size and areal density of the protruding defects were directly associated with the thickness of the Er-silicate layer (Figures S1 and S2 in the Supporting Information). Because the volume expansion occurs on top of the $ErSi_{2-x}$ film, there may be more possibility of buckling in an upward direction on the Si substrate. As explained by Tan et al.,[9] the filling of the underlying voids with regrown defective Si shown in the TEM image in Figure 6b can be explained by the surface energy effect.

4. CONCLUSION

The effect of Ta and TaN capping layers with thicknesses of ∼20 nm and showing different degrees of oxygen permeability on the phase evolution and defect formation during the temperature-dependent silicidation reaction was studied. For the TaN-capped sample, only Si out-diffusion occurred without oxygen incorporation, which followed an ideal silicide-forming path involving nucleation and growth of a crystalline $ErSi_{2-x}$ film, preceded by amorphous Er−Si layer formation (300−500 °C), and crystallinity improvement at up to 700 °C. In the case of the sample capped with somewhat oxygen-permeable Ta, counteracting oxygen in-diffusion from the annealing atmosphere resulted in the formation of crystalline Er_2O_3 and amorphous Er-silicate layers on $ErSi_{2-x}$, and hindered $ErSi_{2-x}$ growth at around 500 °C. A further increase in the annealing temperature induced a continuous growth of the Er-silicate layer by consuming the preformed Er_2O_3 and $ErSi_{2-x}$ layers.

In terms of the surface defects, both the TaN-capped and Ta-capped samples produced a high density of small recessed defects at relatively low annealing temperatures (>∼400 °C), which was probably due to the locally enhanced Si out-diffusion between ultrathin $ErSi_{2-x}$ islands. However, as the annealing temperature was further increased, the different microstructural evolution incurred different forms of dominant surface defects: either recessed or protruding rectangular or square-shaped large defects. The TaN-capped sample with minimal oxygen intrusion exhibited further growth of the recessed defects, which was attributed to the continuous growth of the $ErSi_{2-x}$ film. When a significant amount of oxygen was incorporated, as is in the Ta-capped sample, the formation of amorphous Er-silicate is believed to mainly induce a biaxial compressive film stress and to form a pyramid-like defect shape.

Lastly, although the identity of the capping materials used in this experiment exhibited totally different microstructural and defect evolution, it should be noted that other parameters such as the film thicknesses (of the capping and Er films) and the annealing atmosphere may also play critical roles in controlling the amount of detrimental oxygen diffusion.

■ ASSOCIATED CONTENT

Supporting Information

Cross-sectional TEM and surface SEM images of Ti-capped and TiN-capped Er films on Si in comparison with those of Ta-capped sample after annealing at different temperatures. This information is available free of charge via the Internet at http://pubs.acs.org/.

■ AUTHOR INFORMATION

Corresponding Author

*E-mail: hsubkim@skku.edu.

Notes

The authors declare no competing financial interest.

■ ACKNOWLEDGMENTS

This work was supported by the IT R&D program of MKE/KEIT (Grant 10039174, Technology Development of 22 nm level Foundry Devices and PDK).

■ REFERENCES

(1) Besser, P. R.; Lavoie, C.; Murray, C.; D'Emic, C.; Ohuchi, K. *ECS Trans.* **2008**, *13*, 377−388.
(2) Huda, M. Q.; Sakamoto, K. *Mater. Sci. Eng. B.* **2002**, *89*, 378−381.
(3) Jang, M.; Kim, Y.; Shin, J.; Lee, S.; Park, K. *Appl. Phys. Lett.* **2004**, *84*, 741−743.
(4) Reckinger, N.; Tang, X.; Bayot, V.; Yarekha, D. A.; Dubois, E.; Godey, S.; Wallart, X.; Larrieu, G.; Łaszcz, A.; Ratajczak, J.; Jacques, P. J.; Raskin, J.-P. *J. Appl. Phys.* **2008**, *104*, No. 103523.
(5) Reckinger, N.; Tang, X.; Bayot, V.; Yarekha, D. A.; Dubois, E.; Godey, S.; Wallart, X.; Larrieu, G.; Łaszcz, A.; Ratajczak, J.; Jacques, P. J.; Raskin, J.-P. *Appl. Phys. Lett.* **2009**, *94*, No. 191913.
(6) Reckinger, N.; Tang, X.; Godey, S.; Dubois, E.; Laszcz, A.; Ratajczak, J.; Vlad, A.; Dutu, C. A.; Raskin, J.-P. *J. Electrochem. Soc.* **2011**, *158*, H715−H723.
(7) Reckinger, N.; Duţu, C. A.; Tang, X.; Dubois, E.; Yarekha, D. A.; Godey, S.; Nougaret, L.; Łaszcz, A.; Ratajczak, J.; Raskin, J.-P. *Thin Solid Films* **2012**, *520*, 4501−4505.
(8) Ratajczak, J.; Łaszcz, A.; Czerwinski, A.; Katcki, J.; Phillipp, F.; Van Aken, P. A.; Reckinger, N.; Dubois, E. *J. Microsc.* **2010**, *237*, 379−383.
(9) Tan, E. J.; Bouville, M.; Chi, D. Z.; Pey, K. L.; Lee, P. S.; Srolovitz, D. J.; Tung, C. H. *Appl. Phys. Lett.* **2006**, *88*, 021908.
(10) Tan, E. J.; Pey, K. L.; Chi, D. Z.; Lee, P. S.; Tang, L. J. *IEEE Electron Device Lett.* **2006**, *27*, 93−95.
(11) Luo, C. H.; Chen, L. J. *J. Appl. Phys.* **1997**, *82*, 3808−3814.
(12) Huang, W.; Ru, G. P.; Jiang, Y. L.; Qu, X. P.; Li, B. Z.; Liu, R. *Thin Solid Films* **2008**, *516*, 4252−4257.
(13) Tsai, W. C.; Chi, K. S.; Chen, L. J. *J. Appl. Phys.* **2004**, *96*, 5353−5356.
(14) Wu, C. S.; Lau, S. S.; Kuech, T. F.; Liu, B. X. *Thin Solid Films* **1983**, *104*, 175−182.
(15) Knapp, J. A.; Picraux, S. T.; Wu, C. S.; Lau, S. S. *J. Appl. Phys.* **1985**, *58*, 3747−3757.
(16) Lau, S. S.; Pai, C. S.; Wu, C. S.; Kuech, T. F.; Liu, B. X. *Appl. Phys. Lett.* **1982**, *41*, 77−80.
(17) Tan, E. J.; Kon, M. L.; Pey, K. L.; Lee, P. S.; Zhang, Y. W.; Wang, W. D.; Chi, D. Z. *Thin Solid Films* **2006**, *504*, 157−160.
(18) Queralt, X.; Ferrater, C.; Sánchez, F.; Aguiar, R.; Palau, J.; Varela, M. *Appl. Surf. Sci.* **1995**, *86*, 95−98.
(19) Shen, G. H.; Chen, J. C.; Lou, C. H.; Cheng, S. L.; Chen, L. J. *J. Appl. Phys.* **1998**, *84*, 3630−3635.
(20) Travlos, A.; Salamouras, N.; Boukos, N. *J. Phys. Chem. Solids* **2003**, *64*, 87−93.
(21) Peng, G. W.; Feng, Y. P.; Huan, A. C. H.; Bouville, M.; Chi, D. Z.; Srolovitz, D. J. *Phys. Rev. B* **2007**, *75*, 125319.
(22) Yang, J. J.; Rawn, C. J.; Ji, C.-X.; Chang, Y. A.; Chen, Y.; Ragan, R.; Ohlberg, D. A. A.; Williams, R. S. *Appl. Phys. A: Mater. Sci. Process.* **2006**, *82*, 39−42.
(23) Dargis, R.; Williams, D.; Smith, R.; Arkun, E.; Roucka, R.; Clark, A.; Lebby, M. *ECS J. Solid State Sci. Technol.* **2012**, *1*, N24−N28.